Journal of Materials Chemistry C

Accepted Manuscript

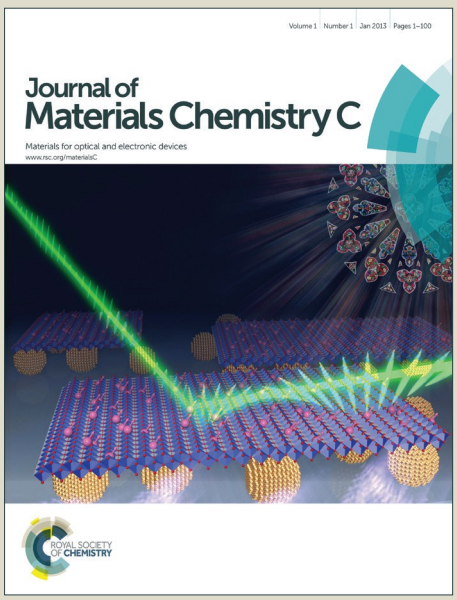

ROYAL SOCIETY OF CHEMISTRY

www.rsc.org/materialsC

Journal Name

ARTICLE

How to induce highly efficient long-lasting phosphorescence in a lamp used commercial phosphor: a facile method and fundamental mechanisms

Received 00th January 20xx,
Accepted 00th January 20xx

DOI: 10.1039/x0xx00000x

www.rsc.org/

Zehua Zou,[a] Jing Wu,[a] Jiachi Zhang*[a], Zhipeng Ci*[a] and Yuhua Wang[a]

We successfully tailor the properties of a well-known commercial lamp used $Zn_2SiO_4:Mn^{2+}$ phosphor as a novel, highly efficient, long-lasting green phosphor with the co-doping method. The long-lasting phosphorescence (LLP) of the optimal $Zn_2SiO_4:Mn^{2+},Yb^{3+}$ sample can be recorded for approximately 30 h (0.32 mcd/m^2) and is visible for even more than 60 h in dark by using dark-adapted vision. This exciting result is sufficiently encouraging for the initiation of a more thorough investigation. Several classical methods of investigation including decay curves, thermoluminescence, fading experiments, multi-peak fitting based on general-order kinetics, and first-principle calculations are used in this study to examine the LLP properties, the effects of such co-dopants and the nature of traps in detail. The important retrapping and tunneling effects, combined with a kinetics investigation, are discussed. A modified law concerning the influences of co-dopants on the traps around the Mn^{2+} (3d5, d→d type) centers and the LLP properties are summarized. Finally, the LLP mechanism of the $Zn_2SiO_4:Mn^{2+},Yb^{3+}$ phosphor is proposed.

1 Introduction

Some photoluminescent materials are able to continue emitting visible light for minutes or hours after excitation has ended, a phenomenon known as long-lasting phosphorescence (LLP).[1-5] The first record of an LLP material, which was found in nature, was during the Song Dynasty of China (11th century A.D.).[6] In 1602, Italian Vincenzo Casciarolo discovered the famous Bolognian stone, which could emit blue-violet light for a few minutes in darkness.[7] In 1671, the origin of the LLP phenomenon was revealed to be the impurity-type luminescence of barium sulfide (BaS) when the mineral is heated with carbon black.[8] For more than a century, sulfides have been used as LLP phosphors and widely investigated as luminescent host lattices as well. However, it is well known that sulfide phosphors are not sufficiently stable and bright for many practical applications. Although numerous LLP materials have been previously reported, it was only in 1996 that this field of research began to attract much wider interest due to the discovery of the highly bright LLP of $SrAl_2O_4:Eu^{2+},Dy^{3+}$ phosphor by Matsuzawa et al.[9] Currently, LLP materials are extensively applied in emergency lighting, safety signage,[10] optical storage media,[11,12] in vivo imaging,[1,13] drug carriers,[14] solar energy,[15] and even photocatalysis.[16,17]

At present, the best performances of LLP materials are still exhibited by Eu^{2+}-doped alkali-earth aluminate phosphors such as $SrAl_2O_4:Eu^{2+},Dy^{3+}$ (green, >30 h)[9] and $CaAl_2O_4:Eu^{2+},Nd^{3+}$ (blue, >10 h).[18] During the past decades, a large number of new LLP phosphors have been developed. Numerous groups have made good progress on development of green LLP phosphors, as shown in Table S1.[4,6,19-35] However, $SrAl_2O_4:Eu^{2+},Dy^{3+}$, which exhibits a bright-green LLP that remains visible for more than 30 h with dark-adapted vision, is still the most important and studied LLP phosphor up to now. Nonetheless, alkali-earth aluminates are not sufficiently stable under acid or alkaline conditions, and the Eu^{2+} centers are easily oxidized, thereby resulting in continuous LLP degradation. Furthermore, the LLP mechanism remains unclear thus far and this limits the development of these materials. Therefore, it is necessary to continue the development of new LLP phosphors for obtaining improved applications and a more precise understanding of the LLP mechanism.

For the development of a new LLP material, researchers often must choose a previously unreported host to ensure so-called "novelty" through a trial and error method. By using this inefficient method, some researchers may be fortunate enough to discover LLP phenomena in a new material, but this result is not guaranteed. In fact, most researchers generally fail to observe LLP phenomena in many new materials or even find a highly efficient example. Therefore, we must reject this inefficient method, which is founded on trial and error. Furthermore, it may be beneficial to develop a new LLP material by tailoring the properties of existing highly efficient commercial lighting or displays used phosphors. Accordingly, J. Ueda has successfully developed a new blue-light-excited, yellow-green LLP phosphor (>20 h) based on commercial light-emitting diodes (LEDs) used $Y_3Al_5O_{12}:Ce^{3+}$ (YAG) phosphor.[36] Moreover, our group has also obtained a yellow-red LLP phosphor

[a] Key Laboratory for Magnetism Magnetic Materials of the Ministry of Education, Lanzhou University, Lanzhou 730000, P.R. China.

† Footnotes relating to the title and/or authors should appear here.
Electronic Supplementary Information (ESI) available: [details of any supplementary information available should be included here]. See DOI: 10.1039/x0xx00000x

that can last for more than 47 h based on commercial plasma display panels (PDPs) used red borate phosphor.[10] Furthermore, Xie recently reported a novel red LLP phosphor, Y_2O_3:Eu^{3+},Ho^{3+}, which was originally developed for use only a few months ago in a well-known commercial fluorescent lamp used Y_2O_3:Eu^{3+} phosphor.[37]

It is important to consider our options in this work. It is well known that manganese-doped zinc orthosilicate, Zn_2SiO_4:Mn^{2+}, is a very important material extensively used as a green phosphor in cathode ray tubes (CRTs), fluorescent lamps, and plasma display panels because of its highly efficient photoluminescence (PL), high pure color, long lifespan, chemical stability, and lack of moisture sensitivity.[38] Manganese occurs as Mn^{2+} ions located on two nonequivalent zinc sites in the rhombohedral crystal with tetrahedral site symmetry.[39] Green emission of the material is then ascribed to the $^4T_1$ (^4G)→$^6A_1$ (^6S) spin-flip transition of the Mn^{2+} ($3d^5$) center and, when excited directly in the Mn^{2+} absorption bands, decays exponentially with a decay time of approximately 10 ms.[40] In addition to this intrinsic emission, ultraviolet excitation generates a very weak but relatively long-lived luminescence (i.e., LLP) with the same green spectral distribution. It is apparent that this weak LLP (<5 min) arises from the electron–hole recombination process, suggesting the presence of some proper traps in Zn_2SiO_4:Mn^{2+}. It is well known that the LLP phenomenon requires the presence of abundant proper traps with the capability to intercept free carriers and to immobilize them for an appropriate length of time.[4] Thus, it is expected to further tailor the properties of Zn_2SiO_4:Mn^{2+} as a highly efficient green LLP material.

One method of tailoring the properties of a photoluminescent (PL) material as an LLP phosphor is through the introduction of potential traps or increasing the number of existing traps with proper depth in a phosphor lattice by creating nonstoichiometry (i.e., doping or co-doping). Such an effect is generally achieved by co-doping cations or anions with a charge similar to or different from those of the original lattice constituents. By far the most successful examples employing the co-doping method are the current commercial green and blue LLP phosphors: $SrAl_2O_4$:Eu^{2+},Dy^{3+} and $CaAl_2O_4$:Eu^{2+},Nd^{3+}.[9,18] Clabau has reported that the influence of Ln^{3+} co-dopants on traps around Eu^{2+} is associated with the ionization potentials, which can provide a good explanation for the LLP improvement of Eu^{2+} (5d→4f type).[41] However, LLP generally originates from one of the three prior transitions: 5d→4f, d→d, or 4f→4f. At present, the influence of co-dopants on traps around transition metal ions such as Mn^{2+} ($3d^5$, d→d type) is still unclear and lacks systematic experimental investigation.

In this work, we successfully tailor the properties of a commercial lamp used Zn_2SiO_4:Mn^{2+} material as a novel, highly efficient green LLP phosphor by using the co-doping method. The LLP of the optimal Zn_2SiO_4:Mn^{2+},Yb^{3+} sample can last for about 30 h before it drops below 0.32 mcd/m^2; in particular, it can be observed for more than 60 h with dark-adapted vision. Therefore, this exciting result is sufficient for encouraging a more thorough investigation of the critical role of co-dopants and the physical processes taking place in this material during and after excitation.

2 Experimental

All samples in this work were synthesized by traditional solid-state reactions. The raw materials used include ZnO (AR), SiO_2 (AR), $MnCO_3$ (99.8%), and Yb_2O_3 (99.9%). After the ingredients were mixed thoroughly, the mixtures were fired in alumina crucibles for 6 h at 1350 °C in air and the samples were obtained.

All samples were characterized as single phases through powder X-ray diffraction (XRD) by using a Rigaku D/Max-2400 X-ray diffractometer with Ni-filtered Cu Kα radiation. The PL spectra were obtained by using a FLS-920T fluorescence spectrophotometer with a Xe 900 lamp (450 W). The LLP decay curves were measured with an R305 long afterglow instrument (Zhejiang University Sensing Instrument Co. Ltd.,). The TL glow curves were recorded by an FJ-427A1 meter (Beijing Nuclear Instrument Factory) at a heating rate of 1 K/s.

The Rietveld structure refinement of the Zn_2SiO_4 host was conducted by the general structure analysis system (GSAS) program using the experimental XRD data. The calculations of the electronic structure for all samples were conducted by using the Vienna ab initio simulation package (VASP). The Perdew–Burke–Ernzerhof (PBE) exchange-correlation functional within the generalized gradient approximation (GGA) was selected. The crystal information was based on the refined coordinates of all atoms and the relevant parameters of the Zn_2SiO_4 crystal, as shown in Table 1.

3 Results and discussion

1. Micro-structure and luminescence properties

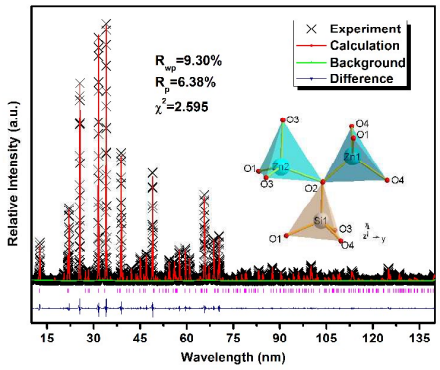

Fig. 1. The Rietveld refinement of the powder XRD profile of the Zn_2SiO_4 host. Inset: the cations in coordination with oxygen atoms.

According to the X-ray diffraction patterns, all samples are good single phases (Fig. S1). The Mn^{2+} and Yb^{3+} ions can replace the two types of Zn^{2+} sites, which are statistically coordinated by four oxygen atoms in the unit cell, as shown in the inset of Fig. 1. In order to provide reliable crystal information of the as-prepared Zn_2SiO_4 samples for first-principles calculations, the Zn_2SiO_4 host was selected to implement Rietveld structure refinement by adopting the GSAS program as shown in Fig. 1. The refinement

factors of the weighted profile *R*-factor (R_{wp}) and the *R* factor (R_p) were 9.30% and 6.38%, respectively, indicating that the refined results are reliable. Table 1 shows the refined coordinates of all atoms and the crystal parameters of Zn_2SiO_4 host.

Table 1. Refined coordinates of all atoms and the unit cell parameters of the Zn_2SiO_4.

Space group		R -3 (148) - trigonal			
Cell		a = b = 13.93590 (13) Å; c = 9.30604 (8) Å			
Sites	x	y	z	Occupancy	Uiso
Zn1	0.9833820(0)	0.1915810(0)	0.4180250(0)	1.000(0)	0.009269
Zn2	0.9728190(0)	0.1898300(0)	0.0839220(0)	1.000(0)	0.009016
Si1	0.9871730(0)	0.1982080(0)	0.7560880(0)	1.000(0)	0.002455
O1	0.1184220(0)	0.2176450(0)	0.7482080(0)	1.000(0)	0.006161
O2	0.0148530(0)	0.3223740(0)	0.7466900(0)	1.000(0)	0.015981
O3	0.9256630(0)	0.1202040(0)	0.8966290(0)	1.000(0)	0.004578
O4	0.9207410(0)	0.1187480(0)	0.1187480(0)	1.000(0)	0.006311

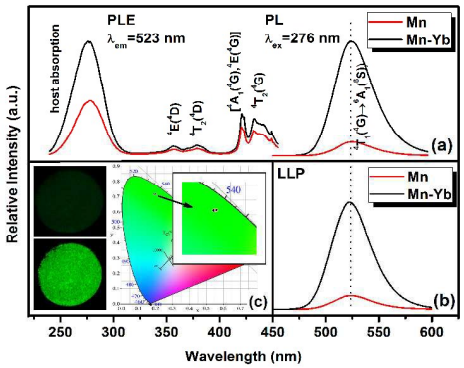

Fig. 2. (a) The PL excitation and emission spectra, (b) the LLP emission spectra recorded at 30 s after UV irradiation for 60 s, (c) the CIE chromaticity coordinates and the images of the Zn2SiO4:0.2%Mn2+ and Zn2SiO4:0.2%Mn2+,1.5%Yb3+ samples.

Fig. 2(a) shows the PL excitation (λ_{em} = 523 nm) and emission (λ_{em} = 276 nm) spectra of the typical Zn_2SiO_4:0.2%Mn^{2+} and Zn_2SiO_4:0.2%Mn^{2+},1.5%Yb^{3+} samples. The optimal contents of Mn^{2+} (0.2%) and Yb^{3+} (1.5%) ions were determined by experiments (Fig. S2). Both samples exhibited an intense excitation band centered at 276 nm and serials of relatively lower peaks at approximately 356 nm, 380 nm, 421 nm, 433nm, due to the transitions from $^6A_1(^6S)$ to $^4E(^4D)$, $^4T_2(^4D)$, $[^4A_1(^4G),^4E(^4G)]$, and $^4T_2(^4G)$ levels of Mn^{2+}, respectively.[42] The former (276 nm) is related to the host absorption (~4.5 eV) and is very strong because it is an allowed transition. The latter is related to direct excitation of 3d electrons from Mn^{2+}, which is forbidden (d→d) and hence is relatively lower. However, the excitation peaks located in the visible region (350–470 nm) still imply that this Zn_2SiO_4:Mn^{2+},Yb^{3+} phosphor may be partially activated by sunlight. Moreover, the broad emission band (470–600 nm) under 276 nm excitation is attributed unambiguously to the transition of $^4T_1(^4G)$ to $^6A_1(^6S)$ of Mn^{2+}. In addition, it is observed that both the PLE and PL intensity were enhanced greatly by Yb^{3+} co-dopants. Before Yb^{3+} co-doping, the PL only originates from the direct recombination. But after the incorporation of Yb^{3+} co-dopants, the PL originates from not only the electrons promoted by excitation but also the electrons thermally released from traps. As a result, the Zn_2SiO_4:Mn^{2+},Yb^{3+} sample with efficient LLP would show much higher PLE and PL intensity. Fig. 2(b) shows the LLP spectra of the Zn_2SiO_4:0.2%Mn^{2+} and Zn_2SiO_4:0.2%Mn^{2+},1.5%Yb^{3+} samples, recorded after ultraviolet (UV) irradiation for 60 s and again after a delay of 30 s and it indicates the emission centers are identical in the PL and LLP processes. Fig. 2(c) shows the Commission Internationale de l'Éclairage (CIE) coordinates and the LLP images of the Zn_2SiO_4:0.2%Mn^{2+} (upper) and Zn_2SiO_4:0.2%Mn^{2+},1.5%Yb^{3+} (lower) samples. After UV lamp (254 nm) irradiation for 15min, bright green LLP can be clearly observed in the optimal Zn_2SiO_4:0.2%Mn^{2+},1.5%Yb^{3+} sample, and the CIE coordinates were calculated as (0.2093, 0.7111), which is very close to the standard green coordinates of (0.21, 0.71).

2. Investigation of long-lasting phosphorescence decay curves

As an LLP phosphor, it is necessary to measure the LLP decay curve. Fig. 3 presents the LLP decay curves of the optimal Zn_2SiO_4:0.2%Mn^{2+},1.5%Yb^{3+} sample in (a) linear–linear, (b) single, and (c) double logarithmic diagrams, which were recorded immediately after UV (254 nm) irradiation or artificial sunlight (1000 ± 5% lux) for 15 min. As shown in Fig. 3(a), the LLP intensity decreases quickly at first and then very slowly. It would be of interest to determine the LLP decay model by fitting these curves. Generally, luminescent materials can be classified, according to the decay of their light emission *L*, into two broad categories: those with an exponential decay, $L \propto \exp^{-t/\tau}$, and those with a power law decay $L \propto t^{-m}$. In fact, many materials, particularly those assigned to the latter, display both types of decay behavior.[40] Unlike the exponentially decaying part, in which the rate is determined by the lifetimes of the radiative states, the power law decay rate may be sensitive to the empty emission centers and the filled traps, the latter of which is determined by the rate at which retrapping and recombination occur.[43] Therefore, when the LLP decay appears to be nonexponential, an alternative approach concerning retrapping should be employed.

In previous reports, the LLP decay curves in linear–linear or single logarithmic plots can be fitted exponentially well within the entire time range of the measurement [44,45], as shown in Fig.s 3(a) and (b). However, the decay curves of LLP phosphors should be given on a double logarithmic scale to see the decay processes.[46] As shown in Fig. 3(c), the theoretical formula (function of exponential terms) presents high accuracy in the early rapid-decay stage (t < 1 h), which is due to the low probability of retrapping in this stage: every carrier that thermally escapes a trap can immediately move to Mn^{2+} levels for recombination through the conduction band, and will not be captured by another trap. It would lead to a rapid LLP decay and an exponential LLP decay profile in the early decay stage.[46] However, in the late slow-decay stage (t > 1 h), the exponential fitting of the decay is no longer possible, which means that the retrapping is beginning to work. The retrapping effect is generally associated with a variation of trap depth. As the trapped carriers are released, the trap depth becomes deeper; thus, it becomes more difficult for the carriers to

move to Mn^{2+} levels for recombination through the conduction band. At this stage, a carrier that manages to escape a trap can be immediately captured by another trap, i.e., the retrapping effect. Consequently, the recombination rate of carriers would be slower, leading to much weaker LLP intensity, and therefore, a significantly longer LLP duration time.

On the other hand, the retrapping effect is usually accompanied by the tunneling effect. Fig. 3(d) presents the reciprocal of the LLP intensity as a function of time, i.e., $I^{-1} = f(t)$. This relationship is very close to linear (except $t < 1$ h), and the curve decay approximately as t^{-1} has very important implications in the choice of an acceptable retrapping model. In more general terms, the intensity of LLP may decay according to the I–t^{-a} dependence, with a usually varying between 0.5 and 1 and sometimes even reaching 2.[47] It appears that the linear dependence of I versus t^{-a} is also a sign that LLP occurs through a tunneling-related process. Based on Avouris, the tunneling process in Zn_2SiO_4:Mn^{2+},Yb^{3+} can be described:[40] In the late slow-decay stage ($t > 1$ h), because the trap depth is sufficiently deep, the trapped electrons no longer move to Mn^{2+} through conduction band but are thermally promoted into the shallow tunneling state before being tunneled to the excited state of nearby Mn^{2+} ions. Finally, luminescence occurs when this excited state decays radiatively to the ground state. Obviously, the tunneling effect is slow and always occurs alongside the retrapping effect in the late stage of decay. This process can effectively explain the relatively weaker but much longer LLP emitted during the slow-decay process.

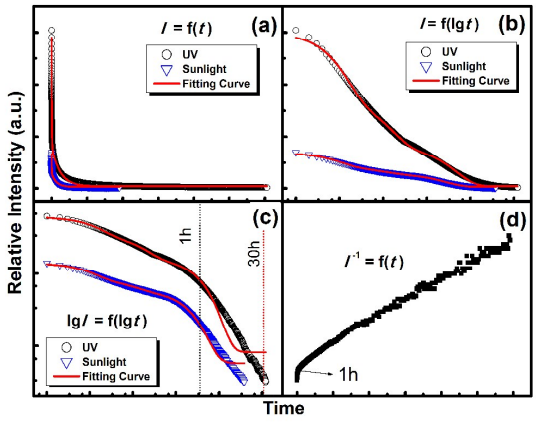

Fig. 3. Decay curves of Zn_2SiO_4:0.2%Mn^{2+},1.5%Yb^{3+} in (a) linear–linear plots, (b) single and (c) double logarithmic plots. (d) LLP intensity in a reciprocal function.

3. Thermoluminescence and fading experiments

It is generally accepted that TL measurement is the most efficient technique used to study the variation of the LLP properties. The positions of TL bands represent the trap depth, whereas lower (higher) temperature corresponds to shallow (deeper) traps.[12] By using the TL technique, it is much easier to evaluate the kinetics, density, and depth of the traps.[48] Fig. 4(a) shows the TL glow curves of the typical Zn_2SiO_4 host and Zn_2SiO_4:0.2%Mn^{2+} and Zn_2SiO_4:0.2%Mn^{2+},1.5%Yb^{3+} samples recorded immediately after UV lamp irradiation for 15 min. Because the TL signal of the Zn_2SiO_4 host was so weak that it produced a nearly straight line, it is also shown alone in Fig. 4(b) for more detail. The Zn_2SiO_4 host clearly exhibited a complex TL glow curve and that three individual TL peaks were located at approximately 342 K, 444 K and 507 K, respectively. It is important to note in Fig. 4(a) that, after a certain amount of Yb^{3+} were co-doped, the TL peak at 342 K shifted slightly to 337 K and was significantly enhanced. Since the TL intensity and position correspond to the density and depth of traps, this result indicates that the Yb^{3+} co-dopants strongly influence the density and depth of the shallow traps and that the shallow traps corresponding to the TL peak at 337 K may play a critical role in the LLP process.

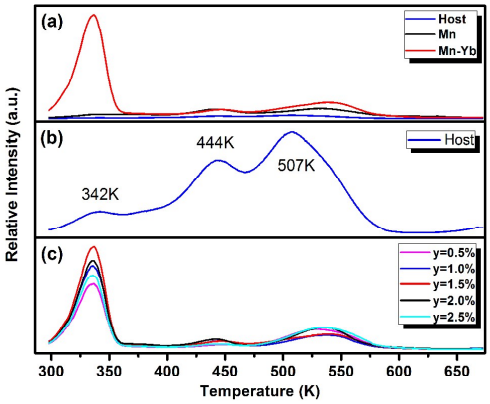

Fig. 4. (a,b) TL of Zn_2SiO_4, Zn_2SiO_4:0.2%Mn^{2+} and Zn_2SiO_4:0.2%Mn^{2+},1.5%Yb^{3+}. (c) TL glow curves of Zn_2SiO_4:0.2%Mn^{2+},y%Yb^{3+} (y = 0.5%, 1.0%, 1.5%, 2.0%, 2.5%).

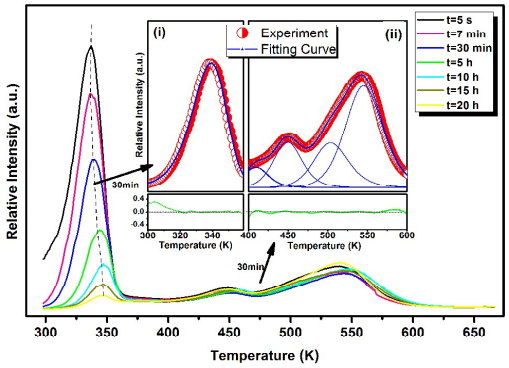

Fig. 5. The TL glow curves of Zn_2SiO_4:0.2%Mn^{2+},1.5%Yb^{3+} at different delay time. Inset: the TL deconvolution and the residue of sample after a 30 min delay at low temperature (i) and middle to high temperature range (ii).

To show the critical role of shallow traps in greater detail, TL fading experiments were conducted in which the TL curves with different delay times were measured after ceasing the UV irradiation. Fig. 5 exhibits the TL glow curves of the optimal Zn_2SiO_4:0.2%Mn^{2+},1.5%Yb^{3+} sample after UV irradiation for 15 min and those after different delay times. As the delay time increased,

the intensity of the TL peak at 337 K gradually decreased, corresponding to the continuous release of trapped carriers in shallow traps. On the contrary, the TL bands at high temperature due to the deep traps did not show clear change during the delay, which indicates that the carriers were strongly immobilized in deep traps at room temperature. Therefore, it concludes that the shallow traps rather than the deep traps are mainly involved in the LLP process at room temperature; thus, changes in shallow traps induced by the Yb^{3+} co-dopants should be mainly responsible for the strong LLP improvement.

Moreover, Fig. 5 also shows that the TL peak due to shallow traps shifted slightly toward the higher temperature. The peak maximum was located at 337 K for the 5 s duration and shifted to 348 K after 20 h. This result indicates that the trap depth is dynamic during the decay process; thus, the distribution of trap depth may be continuous. Furthermore, this slight shift shows that the trap system of the Zn_2SiO_4:Mn^{2+},Yb^{3+} material is more complicated than a single trap obeying first-order kinetics from a Gaussian distribution of trapping levels. Moreover, it further confirms that the retrapping effect cannot be ignored at the late stage of decay.

4. Kinetics of long-lasting phosphorescence process

As was reported in previous research, the ideal trap depth for excellent LLP is at about 0.5–1.2 eV.[46,49,50] To examine the trap depth and the LLP kinetics of the Zn_2SiO_4:Mn^{2+},Yb^{3+}, we introduced a classical multi-peak fitting method developed by Chen et al.[51] Considering that the retrapping effect cannot neglected in this case, the general-order kinetics expression should be utilized to describe the TL glow curves:

$$I(T) = sn_o \exp(-\frac{E}{kT})[1+(b-1)\frac{s}{\beta}\times\int_{T_0}^{T}\exp(-\frac{E}{kT'})dT']^{-\frac{b}{b-1}} \quad , \quad (1)$$

where E is the trap depth (activation energy), and n_0 is the trap concentration of trapped carriers such as electrons and holes at the moment; k is the Boltzmann constant; b is the kinetics order parameter; and β is the heating rate (1 K/s for our experiment). Here, s is the frequency factor. Because it is very difficult to fit a serial of experimental data by a function containing an integral, Equation (1) should be simplified to Equation (2) according to Kitis,[52] and the convenient parameters of I_m, T_m, s, and n_0 can be introduced in the following equations:

$$I(T) = I_m b^{\frac{b}{b-1}}\exp(\frac{E}{kT}\frac{T-T_m}{T_m})\times[(b-1)(1-\Delta)\frac{T^2}{T_m^2}\exp(\frac{E}{kT}\frac{T-T_m}{T_m})+Z_m]^{-\frac{b}{b-1}}, \quad (2)$$

$$s = \frac{\beta E}{kT_m^2}\frac{1}{Z_m}\exp(\frac{E}{kT_m}), \quad (3)$$

$$n_0 = \frac{kT_m^2}{\beta E}I_m Z_m(\frac{b}{Z_m})^{\frac{b}{b-1}}, \quad (4)$$

with $\Delta = \frac{2kT}{E}$ and $Z_m = 1+(b-1)\frac{2kT_m}{E}$,

where I_m is the glow-peak maximum intensity, T_m is the temperature at the maximum, and t_n is the theoretical decay time at T_n K:[53]

$$t_n = \frac{1}{s}\exp(\frac{E}{kT_n}). \quad (5)$$

To explain the kinetics of LLP process during the delay, all of the TL glow curves in Fig. 5 have been fitted, and the deconvolution of the TL curve of the optimal sample after a 30 min delay is given in the inset (Fig. 5i) as a representative. It is found that the dominant TL peak at 337 K due to shallow traps can be fitted well (upper curve), and the small residues (lower curve) indicate that the fitting is reliable. Accordingly, all the calculated TL parameters are exhibited in Table 2.

Table 2. Fitting parameters of TL peak at low temperature after different delay times.

Delay time	E (eV)	b	s (s^{-1})	n_0 (cm^{-3})	t_n (s)
5 s	0.968	1.107	2.727×10^{13}	4.978×10^{7}	832.935
30 min	1.017	1.222	1.133×10^{14}	3.298×10^{7}	1348.952
10 h	1.199	1.260	2.535×10^{16}	8.865×10^{6}	7170.481
20 h	1.201	1.669	3.147×10^{16}	3.096×10^{6}	6241.987

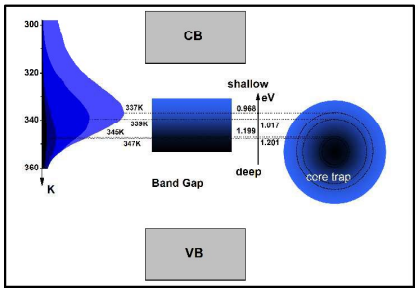

Fig. 6. The schematic of the model of trap in simple terms.

As previously mentioned, an increase in delay time would result in decreases in the intensity of TL peak at 337 K due to shallow traps in addition to a slight shift toward higher temperature. Correspondingly, Table 2 shows that as the delay time increases, the density of trapped carriers (n_0) gradually decreases whereas the trap depth (E) is increased. This result suggests that the continuous distribution of trap depth is clearly associated with the density of trapped carriers. Here, we temporarily propose a simple model of trap in Fig. 6 in which an empty trap can be considered as a point defect. This empty trap can strongly attract the free carriers of opposite charge; this process is known as “trapping”. The carriers gather around the “core” similar to an electron cloud. Then, they are released by thermal energy at room temperature and recombine via a fluorescence mechanism at nearby emission centers; this process is known as “de-trapping.” At the beginning, the outer captured carriers can escape relatively easily by thermal energy; thus, the trap depth at this moment is “shallow”. As the de-trapping continues, it becomes more difficult for the inner carriers to escape; thus, the trap depth is relatively “deep” at this stage. According to this model, it is understandable that the trap depth (E) is dynamic and is strongly dependent on the density of trapped carriers (n_0). The decrease of n_0 results in the increase of

E, and thus the TL peak correspondingly shifts to higher temperature, as shown in Fig. 5.

It is also important to note that in Table 2, although the density of trapped carriers (n_0) decreases rapidly at the beginning, the reduction rate is gradually slowed as the delay time increases. This observation should be associated with the deeper trap depth in addition to the more active retrapping effect. Generally, the retrapping effect can be evaluated by using the kinetics order parameter *b*: *b* equal to 1 is direct recombination, and *b* greater than 1 indicates retrapping. It is clear that as the delay time increased, the kinetic order parameter *b* varied from 1.107 to 1.669, proving that the retrapping of the carriers became increasingly active during the delay. The trapped carriers would be released and then recombine for LLP at far lower rates than those in early stage due to the active retrapping effect, leading to a significantly lower LLP intensity and longer LLP time. Correspondingly, Table 2 also shows that the theoretical decay time (t_n) at 298 K trends to increase from 832 s to 6241 s. Therefore, the retrapping effect is indeed very important for excessively long LLP durations in materials.

5. Electronic structures

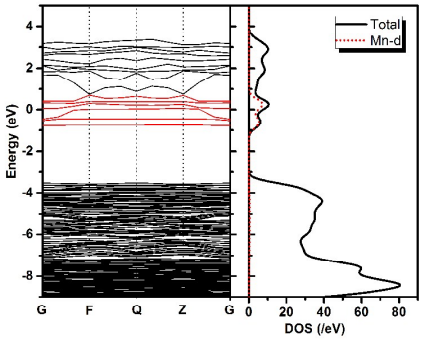

Fig. 7. The band structure, total and partial densities of states of Zn_2SiO_4:Mn^{2+}.

Because the LLP mechanism is closely related to the electronic properties of the emission center and the intrinsic/extrinsic defects acting as trap centers, it is necessary to gain insight into the electronic properties of the host and the emission center. Fig. 7 depicts the computed band structure and total and partial densities of states, respectively, of the Zn_2SiO_4:Mn^{2+} sample. Because of the well-known limitation of GGA–PBE in predicting band gaps, the band gap has been corrected by a scissor value (2.537 eV) based on the absorption spectra of Zn_2SiO_4 (Fig. S3). And only the substitution of Zn−1 sites by Mn^{2+} ions is considered in this calculation for lower formation energy and better stability of defects ($L_{Zn1\text{-}O}$=1.9632 Å, $L_{Zn2\text{-}O}$=1.9212 Å). The impurity levels (red dots) stem from Mn 3d orbitals and the Fermi level lies in the broad impurity levels, suggesting that the ground states of the impurity levels are occupied by electrons and that the excited states are empty. It is significant that the empty 3d excited levels were located within the conduction bands of the host. This finding is significant because the excited levels are above the conduction band; the electrons in excited levels can easily be transferred into the low-conduction bands and can then move to other locations in the crystal. Some of these electrons may be trapped if empty defect (trap) levels exist just below the conduction band. The electrons can remain for a while in the shallow trap and can then be released back into the conduction band. Once nearly free electrons in the conduction band move to the site of Mn^{2+}, they may move into the excited levels of Mn 3d orbitals because the energy difference between the Mn 3d levels and the conduction band is sufficiently small. Consequently, the LLP arises.

This significant finding is also helpful in the discussion on the nature of the traps. Generally, with respect to the intrinsic defects in Zn_2SiO_4 crystal, the high annealing temperatures may create O, Zn, and Si vacancies (V_O, V_{Zn}, and V_{Si}) and interstitial oxygen atoms (O_i). First, we cannot exclude the presence of interstitial oxygen atoms (O_i) because the synthesis atmosphere is air. Silicon vacancies (V_{Si}) may exist as well, but would be energetically unfavorable because the Si–O bonds are short and strong. Therefore, negatively charged O_i and V_{Zn} may be the major hole trap, whereas the only positively charged V_O is expected to serve as the electron trap center.

Because the empty 3d excited levels of Mn^{2+} are just within the conduction band, the excited electrons can easily move to the conduction band. Therefore, some empty electron trap levels should exist below the conduction band minimum so that the free electron carriers in conduction band can be trapped for a while. To capture the free electrons, the empty traps should be positively charged; V_O appears to be the only such candidate in the Zn_2SiO_4 crystal. Considering that there are at least four types of oxygen sites in the Zn_2SiO_4 crystal and that each Zn site is coordinated by three types of these sites (Fig. 1), the three individual TL peaks of the Zn_2SiO_4 crystal shown in Fig. 5 may be related to the intrinsic V_O at different sites. However, the accurate attribution of TL bands remains an open question; concrete evidence for these assumptions is still lacking at this stage.

On the other hand, the transition metal ion such as Cu^+ ($3d^{10}$) and Mn^{2+} ($3d^5$) can be ionized into Cu^{2+} and Mn^{3+}, respectively. Under excitation, one of their electrons can be easily released toward the host and become trapped by anion vacancies. Therefore, the presence of proper electron traps is extremely important for LLP of Mn^{2+}, and thus it is believed that V_O in Zn_2SiO_4 plays a critical role as electron trap to store energy.

6. Role of the Yb^{3+} co-dopants

At this stage, the method in which the Yb^{3+} co-dopants influence the traps in Zn_2SiO_4:Mn^{2+} and therefore improve the LLP performances remains unclear. Generally, an anion vacancy requires some electron density to gain stability. Thus, it is important to consider the abilities of the surrounding cations to delocalize their electron densities toward the vacancy. The ionization potential of a cation (such as $Zn^{2+} \rightarrow Zn^{3+} + e^-$) would be an appropriate parameter to gain insight into its ability to reorganize its electron cloud toward the anion vacancy (V_O in this case).[41] The lower the ionization potential of the cation, the greater the ability of the cation to stabilize V_O; the denser V_O is then more likely to be attracted to the cation.

The ionization potentials of Mn^{2+} and Zn^{2+} are 33.7 eV and 39.8 eV, respectively. Because the ionization potential of Mn^{2+} is clearly lower than that of Zn^{2+}, the V_O would move closer to the

Mn^{2+} cations, thereby becoming electron traps. Clabau determined that if the activator Mn^{2+} and the V_O are too close, the LLP may be diminished for extremely deep depths of traps or the spatial extension of 3d orbitals.[41] Consequently, the LLP of Mn^{2+} single doped Zn_2SiO_4 is very weak for the strong interaction between Mn^{2+} and V_o. To further improve the LLP, the influences of Mn^{2+} on V_O should be appropriately weakened. Moreover, the co-doping method should be considered on the basis of the ionization potentials of different co-dopants.

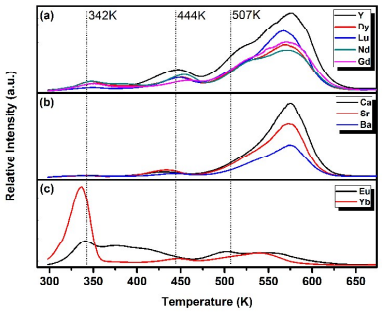

Fig. 8. TL of (a) Y^{3+}, Lu^{3+}, Gd^{3+}, Dy^{3+}, Nd^{3+}; (b) Ca^{2+}, Sr^{2+}, Ba^{2+}; (c) Yb^{3+}, Eu^{3+} co-doped Zn_2SiO_4:Mn^{2+} samples, respectively.

Fig. 8 gives the TL glow curves of the Zn_2SiO_4:Mn^{2+} samples co-doped by (a) Y^{3+}, Lu^{3+}, Gd^{3+}, Dy^{3+}, Nd^{3+}; (b) Ca^{2+}, Sr^{2+}, Ba^{2+}; (c) Yb^{3+}, Eu^{3+} cations. As shown in Fig. 8(a), the TL peak at 507 K shifted to 578 K, and its TL intensity clearly increased by co-doping Y^{3+}, Lu^{3+}, Gd^{3+}, Dy^{3+}, and Nd^{3+}. It is acknowledged that the ionization potentials of Ln^{3+} cations decrease in the order: Y^{3+} (59.6 eV) > Lu^{3+} (45.3 eV) > Gd^{3+} (44.0 eV) > Dy^{3+} (41.4 eV) > Nd^{3+} (40.4 eV) > Mn^{2+} (33.7 eV). This trend is same as that in the TL intensity of the peak at 578 K of Zn_2SiO_4:Mn^{2+},Ln^{3+}. The same trend can be observed in Fig. 8(b), and both the ionization potentials and the intensity of the TL peak at 576 K increased in the order of Ca^{2+} (50.9 eV) > Sr^{2+} (43.6 eV) > Ba^{2+} (36.0 eV) > Mn^{2+} (33.7 eV). It is worthwhile to note that these expectations agree well with the trend in the ionization potentials of ions such that a higher ionization potential relates to a larger density and the deeper depth of deep traps. Although more traps are created, the depth of traps corresponding to the TL peak at 578 K is as large as 1.68 eV, which is too deep for releasing electrons at room temperature; thus, the above Ln^{3+} and alkali-earth metal ions are not useful for the LLP improvement. Correspondingly, because the ionization potentials of Yb^{3+} (43.6 eV) and Eu^{3+} (42.7 eV) ions are obviously larger than that of Mn^{2+} (33.7 eV), it is expected that the Yb^{3+} and Eu^{3+} co-dopants should increase the density and depth of deep traps in a similar manner as the other Ln^{3+} in Fig. 8(a). However, as shown in Fig. 8(c), the density of shallow traps (337 K) rather than deep traps (578 K) is greatly increased, and the depth of shallow traps is slightly reduced, corresponding to the TL shift from 342 K to 337 K. Because additional and sufficiently shallow traps are created, the LLP performances of Zn_2SiO_4:Mn^{2+} are effectively improved by Yb^{3+} and Eu^{3+} co-dopants. This result occurred because the outermost electronic orbitals of Yb^{3+} and Eu^{3+} ions were full or half-filled, and they likely tended to exist in the reduced form Yb^{2+} (Eu^{2+}) in contrast to its Ln^{3+} congeners. The ionization potentials of Yb^{2+} (25.1 eV) and Eu^{2+} (24.9 eV) ions are significantly lower than those of other Ln^{3+} cations and Mn^{2+} (33.7 eV). Although we cannot unequivocally say that Yb^{2+} cations must be present in the as-prepared material, the trend of Yb^{3+} to Yb^{2+} may lead to lower actual ionization potentials of Yb^{3+} than that of Mn^{2+}. As previously mentioned, a lower ionization potential of the co-dopants relates to a greater ability of the co-dopants to stabilize V_O and a higher likelihood that weak V_O are attracted to the emission centers (Mn^{2+}). Therefore, the presence of the Yb^{3+} (with a relatively lower ionization potential than Mn^{2+}) near Mn^{2+} would effectively weaken the influence of Mn^{2+} on V_O. The higher number of V_O in the vicinity of Yb^{3+} cations (i.e., that of electron traps) as well as the slightly weaker interaction between V_O and nearby Mn^{2+} (i.e., the shallower trap depth) lead to the sharp increases in density and a slight reduction in the depth of shallow traps (337 K) for significant improvement in LLP performance. On the contrary, co-doping of cations with larger ionization potentials correspondingly results in higher numbers and deeper depth of the deep traps (578 K). The same was observed in almost all of the other examples. Table 3 shows a summary of the ionization potentials of ions and the influences of co-dopants on the TL peaks previously reported for some phosphors.[23,24,32,54-65] It is obvious that when the ionization potentials of co-dopants such as Yb^{2+}, Eu^{2+}, Sm^{2+}, Tm^{2+} and Zr^{3+} cations are lower than that of Mn^{2+}, the intensity of the TL peak at low temperature is increased and is shifted to a lower temperature. Oppositely, the co-dopants with larger ionization potentials such as Ca^{2+}, Sr^{2+}, Ba^{2+}, and other Ln^{3+} cations would increase the density and depth of deep traps corresponding to the TL bands in a higher temperature region. It is interesting to note that almost all of previous reports that have given the experimental TL spectra can demonstrate this rule. Therefore, our modified rule concerning the influences of co-dopants on traps around Mn^{2+} and LLP performances is actually reliable at this point.

7 Long-lasting phosphorescence mechanism

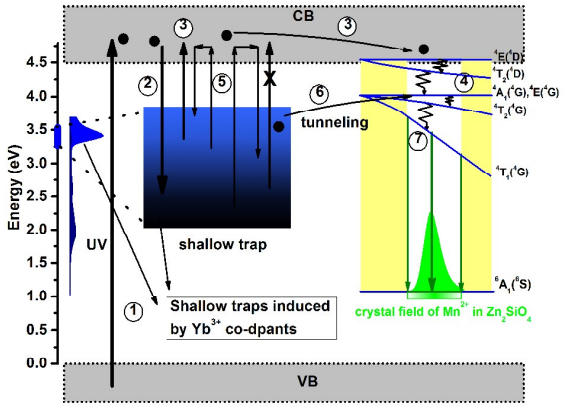

Figure 9. Schematic of LLP mechanism for Zn_2SiO_4:Mn^{2+},Yb^{3+} phosphor.

On the basis of the above results and discussion, the LLP mechanism of this Zn_2SiO_4:Mn^{2+},Yb^{3+} phosphor is proposed in a schematic diagram in Fig. 9. To explain the origin of the broad

emission band of Mn^{2+}, the energy levels of Mn^{2+} in the band gap are given by the slashes based on the Tanabe–Sugano diagram. Under UV lamp excitation, the electrons are promoted to the conduction band (process 1). The electrons are subsequently captured by the shallow traps below the conduction band (process 2). During thermal disturbance at room temperature, the captured electrons are gradually released from the shallow traps which induced by Yb^{3+} co-dopants and are backtracked to the excited levels of 3d orbitals via the conduction band (process 3). Finally, these electrons recombine to generate intense green LLP (process 4). After decay for 1 h, the transfer of electrons through the conduction band is in a much lower rate owing to exhaustion of the outer electrons in the traps. At this point, the retrapping effect, in which free electrons in the conduction band are trapped again by the shallow traps, is more effective (process 5). Moreover, the trapped electrons must be thermally promoted to be located at their shallow tunneling states before tunneling a short distance to arrive at the excited Mn* state (process 6). Finally, this excited state decays radiatively to the ground state of Mn 3d orbitals, generating relatively weak but extra-long LLP (process 7).

Table 3. A summary of the ionization potentials of ions and the influences of co-dopants on TL peaks previously reported for some phosphors.

Phosphors	Activators	IP* (eV)	Codopants	IP* (eV)	TL_s** (K)	TL_c*** (K)	References
$Zn_2SiO_4:Mn^{2+},Yb$			Yb^{2+}	25.1	342, 444, 507	337	This work
$Zn_2SiO_4:Mn^{2+},Ca$			Ca^{2+}	50.9	342, 444, 507	576	This work
$Zn_2SiO_4:Mn^{2+},Y$			Y^{3+}	>51	342, 444, 507	578	This work
$MgGeO_3:Mn^{2+},Yb$			Yb^{2+}	25.1	406	317	54
$Zn_{11}B_{10}Si_4O_{34}:Mn^{2+},Yb$			Yb^{2+}	25.1	375, 470	360	55
$Zn_2GeO_4:Mn^{2+},Yb$			Yb^{2+}	25.1	333, 473, 553	331	23
$MgSiO_3$: Mn^{2+}, Eu			Eu^{2+}	24.9	371, 447, 539	364	56
$CdSiO_3$: Mn^{2+}, Eu			Eu^{2+}	24.9	352	352	57
β -$Zn_3(PO_4)_2:Mn^{2+},Zr$	Mn^{2+}	33.7	Zr^{4+}	33.1	385, 450, 500	344	58
$Zn_2P_2O_7:Mn^{2+},Tm$			Tm^{2+}	23.7	406	340	59
$Zn_{55}Si_{20}B_{50}O_{170}:Mn^{2+},Sm$			Sm^{2+}	23.4	400	340	60
$Zn_3(PO_4)_2:Mn^{2+},Sm$			Sm^{2+}	23.4	420, 470, 530	380	61
$Ca_3(PO_4)_2:Mn^{2+},Dy$			Dy^{3+}	41.4	225	350	62
$CaMgSi_2O_6$: Mn^{2+},Dy			Dy^{3+}	41.4	100-200	480	63
$Ca_9Ln(PO_4)_7:Mn^{2+},Lu$			Lu^{3+}	45.3	130, 180, 220	230	64
$SrAl_2O_4:Mn^{2+},Ce$			Ce^{3+}	36.7	<320	358	32
$Zn_2GeO_4:Mn^{2+}$, Pr			Pr^{3+}	38.9	<320	351	65
$ZnS:Cu^+,Co$	Cu^+	20.3	Co^{2+}	33.6	173	373	24

* IP: ionization potential of ions.

** TL_s: Positions of the TL peaks for the Mn^{2+} single doped phosphor.

*** TL_c: position of the TL peak greatly improved by codopants.

Conclusions

A novel, highly efficient green LLP $Zn_2SiO_4:Mn^{2+},Yb^{3+}$ phosphor is successfully developed by tailoring the properties of a well-known lamp used $Zn_2SiO_4:Mn^{2+}$ phosphor. Its pure green LLP can be measured for approximately 30 and 11 h (0.32 mcd/m^2) after 15 min exposure to UV irradiation and artificial sunlight, respectively. This result reveals that the excellent LLP is attributed to the effective retrapping and tunneling effect in the late slow-decay stage (t > 1 h). The distribution of trap depth is continuous and is related to the density of trapped carriers and the retrapping effect. Accordingly, a simple model of traps similar to an electron cloud is established. First-principle calculations indicate that the empty 3d excited levels of Mn^{2+} are just above the conduction band. Accordingly, the positively charged V_O as shallow electron traps are revealed to be mainly involved in the LLP process. The influences of co-dopants on traps around d→d type Mn^{2+} centers is revealed to be associated with the ionization potentials of co-dopants, and a modified rule is summarized. Finally, the LLP mechanism of this $Zn_2SiO_4:Mn^{2+}$, Yb^{3+} phosphor is proposed.

Acknowledgments

This work was supported by National Nature Science Foundation of China (Nos. 10904057 and 51202099), Fundamental Research Funds for Central Universities (No. Lzjbky-2015-112) and National Science Foundation for Fostering Talents in Basic Research of National Natural Science Foundation of China (Nos. 041105 and 041106).

Notes and references

1 Z. Pan, Y. Y. Lu and F. Liu, *Nat. Mater.*, 2012, **11**, 58-63.
2 B. Qu, B. Zhang, L. Wang, R. Zhou and X. C. Zeng, *Chem. Mater.*, 2015, **27**, 2195-2202.

3 F. Liu, Y. Liang and Z. Pan, *Phys. Rev. Lett.,* 2014, **113***,* 117401.
4 T.-P. Joanna, J. Niittykoski, J. Hölsä and E.Zych, *Chem. Mater.,* 2008, **20***,* 2252-2261.
5 D. Chen, J. Eur. Ceram. Soc., 2014, **34**, 4069-4075.
6 Y. Liu, J. Kuang, B. Lei and C. Shi, *J. Mater. Chem.*, 2005, **15**, 4025-4031.
7 A. Bessière, A. Lecointre, K. R. Priolkar and D. Gourier, *J. Mater. Chem.*, 2012, **22**, 19039-19046.
8 C. Feldmann, T. Jüstel, C. R. Ronda and P. J. Schmidt, *Adv. Funct. Mater.*, 2003, **13**, 511-516.
9 T. Matsuzawa, Y. Aoki, N. Takeuchi and Y. Murayama, *J. Electrochem. Soc.*, 1996, **143**, 2670-2673.
10 W. Zeng, Y. Wang, S. Han, W. Chen, G. Li, Y. Wang and Y. Wen, *J. Mater. Chem. C,* 2013, **1**, 3004-3011.
11 X. Liu, J. Zhang, X. Ma, H. Sheng, P. Feng, L. Shi, R. Hu and Y. Wang, *J. Alloy. Comp.*, 2013, **550**, 451-458.
12 J. Zhang, M. Yu, Q. Qin, H. Zhou, M. Zhou, X. Xu and Y. Wang, *J. Appl. Phys.*, 2010, **108**, 123518.
13 D. Chen, Y. Chen, H. Lu and Z. Ji, Inorg. Chem., 2014, **53**, 8638-8645.
14 A. Abdukayum, J. T. Chen, Q. Zhao and X. P. Yan, *J. Am. Chem. Soc.,* 2013, **135***,* 14125-14133.
15 W. He, T. S. Atabaev, H. K. Kim and Y.-H. Hwang, *J. Phys. Chem. C,* 2013, **117**, 17894-17900.
16 X. Ma, J. Zhang, H. Li, B. Duan, L. Guo, M. Que and Y. Wang, *J. Alloy. Comp.,* 2013, **580**, 564-569.
17 Y. Mei, H. Xu, J. Zhang, Z. Ci, M. Duan, S. Peng, Z. Zhang, W. Tian, Y. Lu and Y. Wang, *J. Alloy. Comp.,* 2015, **622**, 908-912.
18 J. Hölsä, H. Jungner, M. Lastusaari and J. Niittykoski, *J. Alloy. Comp.,* 2001, **323**, 326-330.
19 Y. Jin and Y. Hu, *Mater. Res. Bull.,* 2015, **61**, 16-21.
20 W. Sun, Y. Jia, R. Zhao, H. Li, J. Fu, L. Jiang, S. Zhang, R. Pang and C. Li, *Opt. Mater.,* 2014, **36**, 1841-1845.
21 Y. Luo and Z. Xia, *J. Phys. Chem. C,* 2014, **118***,* 23297-23305.
22 T. Takayama, T. Katsumata, S. Komuro and T. Morikawa, *J. Cryst. Growth,* 2005, **275***,* e2013-e2017.
23 Z. Sun, *Chin. J. Inorg. Chem.,* 2012, **28**, 1229-1233.
24 W. Hoogenstraaten and H. A. Klasens, *J. Electrochem. Soc.,* 1953, **100**, 366-375.
25 L. Ma and W. Chen, *J. Phys. Chem. C,* 2011, **115**, 8940-8944.
26 Y. Jin, Y. Hu, L. Chen, X. Wang, G. Ju and Z. Mu, *J. Lumin.,* 2013, **138**, 83-88.
27 P. I. Paulose, J. Joseph, M. K. Rudra Warrier, G. Jose and N. V. Unnikrishnan, *J. Lumin.,* 2007, **127**, 583-588.
28 B. Lei, B. Li, H. Zhang, L. Zhang, Y. Cong and W. Li, *J. Electrochem. Soc.,* 2007, **154**, H623-H630.
29 C. Liu, G. Che, Z. Xu and Q. Wang, *J. Alloy. Comp.,* 2009, **474**, 250-253.
30 B. Lei, B. Li, X. Wang and W. Li, *J. Lumin.,* 2006, **118**, 173-178.
31 J. Wang, M. Zhang, Q. Zhang, W. Ding and Q. Su, *Appl. Phys. B,* 2007, **87**, 249-254.
32 X. Xu, Y. Wang, X. Yu, Y. Li and Y. Gong, *J. Am. Ceram. Soc.,* 2011, **94**, 160-163.
33 X.-J. Wang, D. Jia and W. M. Yen, *J. Lumin.,* 2003, **102**, 34-37.
34 D. Jia, R. S. Meltzer, W. M. Yen, W. Jia and X. Wang, *Appl. Phys. Lett.,* 2002, **80**, 1535-1537.
35 C. Li, Q. Su and S. Wang, *Mater. Res. Bull.,* 2002, **37**, 1443-1449.
36 J. Ueda, K. Kuroishi and S. Tanabe, *Appl. Phys. Lett.,* 2014, **104**, 101904.
37 W. Xie, Y. Wang, C. Zou, J. Quan and L. Shao, *J. Alloy. Comp.,* 2015, **619**, 244-247.
38 J. Liu, Y. Wang, X. Yu and J. Li, *J. Lumin.,* 2010, **130**, 2171-2174.
39 H. K. Perkins, *J. Chem. Phys.,* 1967, **46**, 2398-2401.
40 P. Avouris, *J. Chem. Phys.,* 1981, **74**, 4347-4355.
41 F. Clabau, X. Rocquefelte, S. Jobic, P. Deniard, M.-H. Whangbo, A. Garcia and T. L. Mercier, *Chem. Mater.,* 2005, **17**, 3904-3912..
42 R. Ye, H. Ma, C. Zhang, Y. Gao, Y. Hua, D. Deng, P. Liu and S. Xu, *J. Alloy. Comp.,* 2013, **566**, 73-77.
43 W. L. Medlin, *Phys. Rev.,* 1961, **122***,* 837-842.
44 J. Xu, Z. Ju, X. Gao, Y. An, X. Tang and W. Liu, *Inorg. Chem.,* 2013, **52**, 13875-13881.
45 B. Lei, H. Zhang, W. Mai, S. Yue, Y. Liu and S.-q. Man, *Solid State Sci.,* 2011, **13**, 525-528.
46 K. Van den Eeckhout, A. J. J. Bos, D. Poelman and P. F. Smet, *Phys. Rev. B.,* 2013, **87**, 045126.
47 D. Jia and W. M. Yen, *J. Lumin.,* 2003, **101**, 115-121.
48 D. S. Kshatri and A. Khare, *J. Alloy. Comp.,* 2014, **588**, 488-495.
49 L. Wang, Y. Chen, R. Zhou, Y. Xu and Y. Wang, *ECS J. Solid State Sci. Technol,* 2012, **1**, R72-R75.
50 T. Aitasalo, P. Dereń, J. Hölsä, H. Jungner, J. C. Krupa, M. Lastusaari, J. Legendziewicz, J. Niittykoski and W. Stręk, *J. Solid. State. Chem,* 2003, **171**, 114-122.
51 R. Chen, *J. Electrochem. Soc.,* 1969, **116**, 1254-1257.
52 G. Kitisy, J. M. Gomez-Rosz and J. W. N. Tuynx, *J. Phys. D: Appl. Phys,* 1998, **31**, 2636-2641.
53 N. E, Jpn. *J. Appl. Phys.,* 1984, **23**, L755-L757.
54 Y. Cong, B. Li, S. Yue, L. Zhang, W. Li and X.-j. Wang, *J. Electrochem. Soc.,* 2009, **156***,* H272-H275.
55 C. Li, J. Wang, H. Liang and Q. Su, *J. Appl. Phys.,* 2007, **101***,* 113304.
56 L. Lin, C. Shi, Z. Wang, W. Zhang and M. Yin, *J. Alloy. Comp.,* 2008, **466**, 546-550.
57 X. Qu, L. Cao, W. Liu, G. Su, P. Wang and I. Schultz, *Mater. Res. Bull.* 2012, **47**, 1598-1603.
58 J. Wang, Q. Su and S. Wang, *J. Phys. Chem. Solids,* 2005, **66**, 1171-1176.
59 R. Pang, Y. Jia, R. Zhao, H. Li, J. Fu, W. Sun, L. Jiang, S. Zhang,C. Li, and Q. Su, *Dalton T.* 2014, **43**, 9661-9668.
60 C. Li and Q. Su, *Appl. Phys. Lett.* 2004, **85**, 2190-2192.
61 J. Wang, Q. Su and S. Wang, *Mater. Res. Bull.,* 2005, **40**, 590-598.
62 A. Bessière, A. Lecointre, R. A. Benhamou, E. Suard, G. Wallez and B. Viana, *J. Mater. Chem. C,* 2013, **1**, 1252-1259.
63 A. Lecointre, A. Bessière, B. Viana and D. Gourier, *Rediat. Meas.,* 2010, **45**, 497-499.
64 A. Bessière, R. A. Benhamou, G. Wallez, A. Lecointre and B. Viana, *Acta Mater.,* 2012, **60**, 6641-6649.
65 M. Wan, Y. Wang, X. Wang, H. Zhao and Z. Hu, *Opt. Mater.,* 2014, **36**, 650-654.